INTERNATIONAL JOURNAL FOR NUMERICAL METHODS IN ENGINEERING
Int. J. Numer. Meth. Engng. **45**, 1203–1225 (1999)

A PARTICLE-IN-CELL SOLUTION TO THE SILO DISCHARGING PROBLEM

ZDZISŁAW WIĘCKOWSKI*,†,‡, SUNG-KIE YOUN§ AND JEOUNG-HEUM YEON¶

Department of Mechanical Engineering, Korea Advanced Institute of Science and Technology, 373-1, Kusong-dong, Yusong-gu, Taejon 305-701, Korea

SUMMARY

The problem of flow of a granular material during the process of discharging a silo is considered in the present paper. The mechanical behaviour of the material is described by the use of the model of the elastic–plastic solid with the Drucker–Prager yield condition and the non-associative flow rule. The phenomenon of friction between the stored material and the silo walls is taken into account—the Coulomb model of friction is used in the analysis. The problem is analysed by means of the particle-in-cell method—a variant of the finite element method which enables to solve the pertinent equations of motion on an arbitrary computational mesh and trace state variables at points of the body chosen independently of the mesh. The method can be regarded as an arbitrary Lagrangian–Eulerian formulation of the finite element method, and overcomes the main drawback of the updated Lagrangian formulation of FEM related to mesh distortion. The entire process of discharging a silo can be analysed by this approach. The dynamic problem is solved by the use of the explicit time-integration scheme. Several numerical examples are included. The plane strain and axisymmetric problems are solved for silos with flat bottoms and conical hoppers. Some results are compared with experimental ones. Copyright © 1999 John Wiley & Sons, Ltd.

KEY WORDS: particle-in-cell-method; finite element method; finite deformations; arbitrary Eulerian–Lagrangian description; silo discharging problem; granular material

1. INTRODUCTION

Motion of a granular material during the silo discharging process is analysed in the paper. The main aim of the analysis is to determine interactions between the stored material and silo walls, and the flow pattern. The problem is interesting for both designers and users. The granular material is treated as continuum in this paper. The elastic–plastic body with the Drucker–Prager yield condition and the non-associative flow rule is used to describe the mechanical behaviour of the

* Correspondence to: Zdzisław Więckowski, Department of Mechanics of Materials, Technical University of Łódź, Al. Politechniki 6, 93-590 Łódź, Poland. E-mail: zwi@kmm-lx.p.lodz.pl
† Current address: Department of Mechanics of Materials, Technical University of Łódź, Al. Politechniki 6, 93-590 Łódź, Poland.
‡ Post-doctoral fellow. Permanent Lecturer, Department of Mechanics of Materials, Technical University of Łódź.
§ Associate Professor
¶ Graduate Student

Contract/grant sponsor: Korea Science and Engineering Foundation

CCC 0029–5981/99/211203–23$17.50

Received 16 February 1998
Revised 27 October 1998

In the past, the problem was analysed under some assumptions leading to significant simplification, or even disregard of the principles of continuum mechanics. Simple expressions for stress and velocity distributions are given, for example by Jenike and Shield [1] and Walters [2].

Recently, the problem has been analysed on the basis of continuum mechanics by several authors. The related initial-boundary value problems are solved using numerical techniques, in particular the finite element method. As pioneering works on this field, those written by Eibl and co-workers [3, 4] should be cited here. In the finite element method, two different descriptions of motion have been used in the analysis of the considered problem: the Eulerian description, and the Lagrangian one. In the Eulerian description, the granular material is treated as a non-classical fluid [3–6]—the analysis is most useful in the case of continuous refilling a silo with the material. When the Lagrangian description is used [6–8], the solid model of the granular material is applied; in this case the whole discharging process can be analysed.

Another approach, based on the discrete element formulation, has been suggested recently by Langston *et al.* [9, 10], where material grains are modelled as spherical and cylindrical particles. This technique seems to be useful when the ratio between the diameters of the silo outlet and the material grain is not high.

In the present paper, the entire process of discharging a silo is analysed. The flow of a granular material in a silo is highly distorted. This causes severe problems in computational modelling of such a process. When the updated Lagrangian formulation of the finite element method is used to describe this large displacement, large strain problem, the original element mesh becomes distorted so significantly that the mesh re-zoning is needed to restore proper shapes of elements [7, 8]. The state fields of mass density, velocities and stresses must be mapped from the distorted mesh to a newly generated one. This mapping is not a straightforward task, and introduces errors. In order to handle large distortions problems, several particle- or point-oriented methods (e.g. the diffusive element, element-free, smoothed hydrodynamics particle, reproducing kernel particle, h–p clouds, finite point methods) have been developed recently [11–20]. Among these methods, the particle-in-cell (PIC) method, introduced originally in fluid dynamics by Harlow and co-workers (see [21] and references therein), has been applied successfully to the problems of solid mechanics by Burgess, Sulsky, Schreyer and co-workers [22–25]. The method is also called a material point method in [25]. On the basis of the material presented in [22–25], the particle-in-cell method is applied to the analysis of flow of a granular material in the present paper, and its use is extended to the frictional contact problem. The particle-in-cell method overcomes the above-mentioned troubles relevant to large distortions because it allows to solve the problem using an arbitrary computational mesh, and trace the history of state variables for particles of the body for its entire deformation process. For each time step, calculations consist of two phases: a Lagrangian phase and a convective one. In the first phase, the computational mesh deforms with the body, and is used to determine the strain increment, and the stresses in the sequel. In the latter phase, the new position of the computational mesh is chosen (particularly, it may be the previous position), and the velocity field is mapped from the particles to the mesh nodes. Nodal velocities are determined using the equation which expresses the equivalence of momentum calculated for the particles and for the computational grid. The method, which can be regarded as an arbitrary Lagrangian–Eulerian formulation (ALE) of the finite element method (see e.g. [26]), not only takes advantages of both the Lagrangian and Eulerian schemes but makes it possible to avoid their drawbacks as well. The triangular mesh with linear shape functions, constant during the whole computational process, is used in the paper. The explicit time-integration scheme is used to solve the dynamic problem. Two cases of material flow are taken into consideration: the plane flow and the axisymmetric one.

The particle-in-cell method seems to be very flexible because of its ALE feature, and its implementation—by extension of a standard finite element program—is relatively easy in comparison with other particle-type methods—these are two main reasons for choosing it as a tool of analysis of the investigated problem.

2. SETTING OF THE PROBLEM

Let us consider a time interval $I=[0,T]$, where $T>0$. Let $\Omega\subset\mathscr{R}^3$ denote the region occupied by the body at time $t\in I$, the boundary, $\partial\Omega$, of which consists of three parts Γ_u, Γ_σ, and Γ_c such that

$$\overline{\Gamma_u}\cup\overline{\Gamma_\sigma}\cup\overline{\Gamma_c}=\partial\Omega,\quad \Gamma_u\cap\Gamma_\sigma=\Gamma_u\cap\Gamma_c=\Gamma_c\cap\Gamma_\sigma=\emptyset$$

Although two-dimensional problems are solved in the paper, the general three-dimensional case is considered throughout this section.

The solution to the problem satisfies the governing relations described in the subsections below.

2.1. Equations of motion

The equations of motion are as follows:

$$\sigma_{ij,j}+\varrho\, b_i-\varrho\, a_i=0\quad\text{on }\Omega$$

where σ_{ij} denotes the Cauchy stress tensor, ϱ is mass density, b_i and a_i are vectors of body forces and acceleration, respectively.

2.2. Constitutive relations

The elastic–plastic material model with the Drucker–Prager yield condition and the non-associated flow rule is applied in the paper to describe the behaviour of the granular material [5]. It is assumed that the material is plastically incompressible, which means that the dilatation of the plastic strains is equal to zero.

Let B denote a convex set of plastically admissible stresses

$$B=\{\tau_{ij}\colon f(\tau_{ij})\leqslant 0\}$$

where the Drucker–Prager yield condition is used for the Cauchy stress tensor

$$f(\sigma_{ij})=q-mp$$

where $m=18\sin\varphi/(9-\sin^2\varphi)$ is a number depending on the angle of internal friction, φ, p and q are stress invariants defined as follows:

$$p=-\tfrac{1}{3}\,\sigma_{ii},\quad q=\sqrt{\tfrac{3}{2}\,s_{ij}\,s_{ij}}$$

where $s_{ij}\equiv\sigma_{ij}+p\,\delta_{ij}$ denotes the deviatoric part of the stress tensor.

The constitutive relations can be written in the form

$$d_{ij}=d_{ij}^{\mathrm{e}}+d_{ij}^{\mathrm{p}}$$

$$d^{\mathrm{e}}_{kl} = A^{-1}_{ijkl}\, \overset{\nabla}{\sigma}_{ij}$$

$$d^{\mathrm{p}}_{ij} = \begin{cases} \dot{\lambda}\, \dfrac{\partial g}{\partial \sigma_{ij}} & \text{if } f(\sigma_{ij}) = 0 \\ 0 & \text{if } f(\sigma_{ij}) < 0 \end{cases}$$

where $\dot{\lambda} \geqslant 0$, and g denotes the plastic potential defined by the relation $g = q$, which means that the material is plastically incompressible. The following notation is used above: $d_{ij} = \frac{1}{2}(\dot{u}_{i,j} + \dot{u}_{j,i})$ is the tensor of deformation rate, d^{e}_{ij} and d^{p}_{ij} are its elastic and plastic parts, respectively,

$$\overset{\nabla}{\sigma}_{ij} = \dot{\sigma}_{ij} - \sigma_{ik}\, \dot{\omega}_{kj} - \sigma_{jk}\, \dot{\omega}_{ki} \tag{1}$$

is the Jaumann stress rate tensor, $\dot{\omega}_{ij} = \frac{1}{2}(\dot{u}_{j,i} - \dot{u}_{i,j})$ denotes the spin tensor,

$$A_{ijkl} = \frac{E}{1+v}\left(\frac{1}{1-2v}\,\delta_{ij}\,\delta_{kl} + \frac{1}{2}\,(\delta_{ik}\,\delta_{jl} + \delta_{il}\,\delta_{jk})\right)$$

is the tensor of elastic constants, where E and v denote the Young modulus and Poisson ratio, respectively.

It should be noted that in the case of very large strains the use of the Jaumann stress rate may lead to unphysical results like oscillatory solution (see [27–29]). Although another choice: the Green–Naghdi rate, for which the above-mentioned deficiency is not observed, is regarded by some researchers as preferable, the Jaumann stress rate is mostly used in engineering practice, for example in soil mechanics (see [30–32]). The main reason of using the Jaumann rate in the present paper is its simpler implementation and lower computational cost in comparison with the Green–Naghdi rate.

2.3. Boundary conditions

It is assumed that the displacements are given on the boundary part Γ_u,

$$u_i = U_i \quad \text{on } \Gamma_u$$

and stresses are known on the part Γ_σ,

$$\sigma_{ji}\, n_j = t_i \quad \text{on } \Gamma_\sigma$$

where t_i is the Cauchy stress vector, and n_i denotes the unit vector outwardly normal to the boundary $\partial\Omega$.

On the remaining part of the boundary, Γ_c, the conditions of unilateral frictional contact are considered. Let $g_N(\mathbf{x})$, where $\mathbf{x} \in \Gamma_c$, denote a distance function defined as the distance between the considered point of the surface and the closest point of the surface of an obstacle body (a silo wall) being in contact with point $\mathbf{x}$ or candidating to this. The frictional contact conditions can be described by the following set of relations (see e.g. [33]):

$$\begin{aligned} g_N \geqslant 0, \quad \sigma_N \leqslant 0, \quad \dot{u}_N\, \sigma_N = 0 \\ f_c(\sigma_N, \boldsymbol{\sigma}_T) \leqslant 0, \quad \dot{u}_{Ti}\, \sigma_{Ti} \leqslant 0 \end{aligned} \tag{2}$$

where the Coulomb friction condition is applied

$$f_c(\sigma_N, \boldsymbol{\sigma}_T) = -\mu|\sigma_N| + \|\boldsymbol{\sigma}_T\| \leqslant 0 \tag{3}$$

σ_N and $\boldsymbol{\sigma}_T$ denote the normal and tangential components of the Cauchy stress vector, respectively, $\sigma_N = \sigma_{ij}\, n_i\, n_j$, $\sigma_{Ti} = \sigma_{kj}\, n_k\, (\delta_{ij} - n_i\, n_j)$, μ is the friction coefficient, u_N and $\mathbf{u}_T$ are the normal and tangential components of the displacement vector, respectively, and $\|\cdot\|$ denotes the Euclidean norm of a vector.

In order to save computation time, in case of existence of a symmetry axis, the following conditions are utilized:

$$u_N = 0, \quad \boldsymbol{\sigma}_T = \mathbf{0}$$

which correspond to the conditions of bilateral frictionless contact between the granular material and the silo wall.

2.4. Initial conditions

The following initial conditions are considered:

$$u_i(0) = u_i^{\mathrm{s}}, \quad \dot{u}_i(0) = 0, \quad \sigma_{ij}(0) = \sigma_{ij}^{\mathrm{s}}$$

where u_i^{s} is the static field of displacements caused by the gravity forces, and σ_{ij}^{s} denotes the corresponding field of stresses.

3. SPACE DISCRETIZATION

As in the standard finite element method, the principle of virtual work is used as the starting point for the formulation of the particle-in-cell method. The equation of virtual work has the following form:

$$\int_\Omega \varrho \left(a_i w_i + \frac{1}{\varrho}\, \sigma_{ij} w_{i,j} \right) \mathrm{d}x = \int_\Omega \varrho b_i w_i \,\mathrm{d}x - \int_{\Gamma_\sigma} t_i w_i \,\mathrm{d}s \quad \forall \mathbf{w} \in V_0 \tag{4}$$

where

$$V_0 = \left\{ \mathbf{w} \in [H^1(\Omega)]^3 :\ w_i = 0 \text{ on } \Gamma_u \right\}$$

where $H^1(\Omega)$ denotes the Sobolev space of functions being square integrable with their derivatives (see e.g. [34, 35]). It should be noted that the space V_0 is chosen for the test function $\mathbf{w}$—the problem of regularity of fields of velocity or displacements, being the solution of the problem, is out of the scope of this paper.

In the particle-in-cell method, two kinds of space discretization are used. Firstly, the region initially occupied by the considered body is divided into a finite number of subregions. Each subregion is represented by one of its points, called a material point. It is assumed that the whole mass of each subregion is concentrated at the corresponding material point, which means that the mass density field is assumed to be distributed as follows:

$$\varrho = \sum_{P=1}^{N} M_P\, \delta(\mathbf{x} - \mathbf{X}_P) \tag{5}$$

where M_P and $\mathbf{X}_P$ are mass and position of the Pth material point, respectively, $\delta(\mathbf{x})$ denotes the Dirac delta function, and N is the number of material points. All state variables like fields of

velocity, mass density, stresses, strains, etc., are traced at the material points which is a distinctive feature for the Lagrangian description of motion. On the other hand, the equation of virtual work is formulated and solved on the computational (Eulerian) mesh. The mesh should cover the virtual position of the analysed body, and can be changed during computations or remain constant.

After applying (5), the equation of virtual work (4) can be written in the form

$$\sum_{P=1}^{N} M_P \left(a_i(\mathbf{X}_P)\, w_i(\mathbf{X}_P) + \sigma_{ij}^{\varrho}(\mathbf{X}_P)\, w_{i,j}(\mathbf{X}_P)\right) = \sum_{P=1}^{N} M_P\, b_i(\mathbf{X}_P)\, w_i(\mathbf{X}_P) + \int_{\Gamma_\sigma} t_i\, w_i \,\mathrm{d}s \tag{6}$$

where $\sigma_{ij}^{\varrho} = \sigma_{ij}/\varrho$. The standard finite element approximation technique is used for fields a_i and w_i. In the case of two-dimensional problems, these two fields can be represented in matrix notation as follows:

$$\mathbf{a}(\mathbf{x},t) \equiv \begin{bmatrix} a_x \\ a_y \end{bmatrix} = \mathbf{N}\mathbf{a}, \quad \mathbf{w}(\mathbf{x},t) \equiv \begin{bmatrix} w_x \\ w_y \end{bmatrix} = \mathbf{N}\mathbf{w} \tag{7}$$

where $\mathbf{N}$ is the matrix of global shape functions defined for the whole computational mesh,

$$\mathbf{N}(\mathbf{x}) = \begin{bmatrix} N_1(\mathbf{x}) & 0 & N_2(\mathbf{x}) & 0 & \dots & N_n(\mathbf{x}) & 0 \\ 0 & N_1(\mathbf{x}) & 0 & N_2(\mathbf{x}) & \dots & 0 & N_n(\mathbf{x}) \end{bmatrix}$$

$\mathbf{a} \equiv [\, a_{1x}\ a_{1y}\ a_{2x}\ \dots\ a_{nx}\ a_{ny}\,]^{\mathrm{T}}$ and $\mathbf{w} \equiv [\, w_{1x}\ w_{1y}\ w_{2x}\ \dots\ w_{nx}\ w_{ny}\,]^{\mathrm{T}}$ are nodal values of fields a_i and w_i, respectively. In the above definitions, n denotes the number of nodes in the computational grid.

Let us consider the plane strain problem and define the following vectors:

$$\mathbf{s}^{\varrho} = \frac{1}{\varrho}\begin{bmatrix} \sigma_{xx} \\ \sigma_{yy} \\ \sigma_{xy} \end{bmatrix}, \quad \mathbf{b} = \begin{bmatrix} b_x \\ b_y \end{bmatrix}, \quad \mathbf{t} = \begin{bmatrix} t_x \\ t_y \end{bmatrix}$$

Applying relations (7) in (6), we obtain the discretized formulation of the problem

$$\mathbf{w}^{\mathrm{T}} \sum_{P=1}^{N} M_P\, \mathbf{N}^{\mathrm{T}}(\mathbf{X}_P)\, \mathbf{N}(\mathbf{X}_P)\, \mathbf{a} + \mathbf{w}^{\mathrm{T}} \sum_{P=1}^{N} M_P\, \mathbf{B}^{\mathrm{T}}(\mathbf{X}_P)\, \mathbf{s}^{\varrho}(\mathbf{X}_P)$$
$$= \mathbf{w}^{\mathrm{T}} \sum_{P=1}^{N} M_P\, \mathbf{N}^{\mathrm{T}}(\mathbf{X}_P)\, \mathbf{b}(\mathbf{X}_P) + \mathbf{w}^{\mathrm{T}} \int_{\Gamma_\sigma} \mathbf{N}^{\mathrm{T}}\, \mathbf{t}\, \mathrm{d}s$$

which means, due to the fact that $\mathbf{w}$ is arbitrary except nodes belonging to Γ_u, that the following system of equations is to be satisfied:

$$\mathbf{M}\mathbf{a} = \mathbf{F} - \mathbf{R} \tag{8}$$

where

$$\mathbf{M} = \sum_{P=1}^{N} M_P\, \mathbf{N}^{\mathrm{T}}(\mathbf{X}_P)\, \mathbf{N}(\mathbf{X}_P)$$
$$\mathbf{F} = \sum_{P=1}^{N} M_P\, \mathbf{N}^{\mathrm{T}}(\mathbf{X}_P)\, \mathbf{b}(\mathbf{X}_P) + \int_{\Gamma_\sigma} \mathbf{N}^{\mathrm{T}}\, \mathbf{t}\, \mathrm{d}s \tag{9}$$
$$\mathbf{R} = \sum_{P=1}^{N} M_P\, \mathbf{B}^{\mathrm{T}}(\mathbf{X}_P)\, \mathbf{s}^{\varrho}(\mathbf{X}_P)$$

Matrix **B** has the same structure like the strain–displacement matrix used in the standard finite element method

$$\mathbf{B}(\mathbf{X}_P) = \begin{bmatrix} \frac{\partial N_1}{\partial x}(\mathbf{X}_P) & 0 & \frac{\partial N_2}{\partial x}(\mathbf{X}_P) & 0 & \dots \\ 0 & \frac{\partial N_1}{\partial y}(\mathbf{X}_P) & 0 & \frac{\partial N_2}{\partial y}(\mathbf{X}_P) & \dots \\ \frac{\partial N_1}{\partial y}(\mathbf{X}_P) & \frac{\partial N_1}{\partial x}(\mathbf{X}_P) & \frac{\partial N_2}{\partial y}(\mathbf{X}_P) & \frac{\partial N_2}{\partial x}(\mathbf{X}_P) & \dots \end{bmatrix}$$

We obtain the same system of equations (8) for the axisymmetric problem, if we use the variables (x, y, Θ) instead of (r, z, Θ), the following representation for mass density:

$$\varrho = \sum_{P=1}^{N} M_P \frac{1}{2\pi x} \delta(\mathbf{x} - \mathbf{X}_P)$$

and the following definitions for vector $\mathbf{s}^{\varrho}$ and matrix **B**:

$$\mathbf{s}^{\varrho} = \frac{1}{\varrho} \begin{bmatrix} \sigma_{xx} \\ \sigma_{yy} \\ \sigma_{xy} \\ \sigma_{\Theta\Theta} \end{bmatrix}, \quad \mathbf{B} = \begin{bmatrix} \frac{\partial N_1}{\partial x}(\mathbf{X}_P) & 0 & \frac{\partial N_2}{\partial x}(\mathbf{X}_P) & 0 & \dots \\ 0 & \frac{\partial N_1}{\partial y}(\mathbf{X}_P) & 0 & \frac{\partial N_2}{\partial y}(\mathbf{X}_P) & \dots \\ \frac{\partial N_1}{\partial y}(\mathbf{X}_P) & \frac{\partial N_1}{\partial x}(\mathbf{X}_P) & \frac{\partial N_2}{\partial y}(\mathbf{X}_P) & \frac{\partial N_2}{\partial x}(\mathbf{X}_P) & \dots \\ \frac{N_1}{x}(\mathbf{X}_P) & 0 & \frac{N_2}{x}(\mathbf{X}_P) & 0 & \dots \end{bmatrix}$$

The effect of frictional contact can be accounted for in equation (8) by adding the vector of contact forces, $\mathbf{F}_c$, to the right-hand side of the equation, i.e.

$$\mathbf{Ma} = \mathbf{F} + \mathbf{F}_c - \mathbf{R} \tag{10}$$

Because of the Dirac delta function representation of the mass density, the mass matrix is singular when its consistent form is considered. To solve system (10), the diagonalized matrix, $\mathbf{M}_l$, or nearly consistent matrix, $\mathbf{M}_\alpha = \alpha \mathbf{M} + (1-\alpha)\mathbf{M}_l$, can be used instead of **M**, where $0 \leqslant \alpha < 1$ [22]. The diagonalized matrix is employed in this paper.

4. TIME INTEGRATION OF THE DYNAMIC PROBLEM

The solution to the dynamic system (10) is found for a discrete set of instants $t_1, t_2, \dots, t_k, \dots \in I$ $(0 < t_1 < t_2 < \cdots < t_k \cdots < T)$, by the use of the explicit procedure of time integration. For each time increment, the calculations consist of two steps: a Lagrangian step and a convective one.

In the Lagrangian step, the calculations are performed in a similar way as in the updated Lagrangian formulation of the standard finite element method—it is assumed that the computational mesh deforms together with the considered body. The state variables are calculated for each material point by using shape functions and nodal parameters defined on the computational mesh. For example, the velocity vector for the Pth material point, $\mathbf{V}_P \equiv [V_{Px}\ V_{Py}]^{\mathrm{T}}$, is obtained from the equation

$$\mathbf{V}_P = \mathbf{N}(\mathbf{X}_P)\, \mathbf{v}^{\mathrm{e}}$$

where $\mathbf{v}^{\mathrm{e}} = [\, v_{1x}\ v_{1y}\ v_{2x}\ v_{2y}\ \ldots\ v_{n_{\mathrm{e}}x}\ v_{n_{\mathrm{e}}y}\,]^{\mathrm{T}}$ is the vector of the nodal velocities of the element which the material point belongs to. The vector of strain increment can be calculated using matrix $\mathbf{B}$ as follows:

$$\Delta\mathbf{e} = \Delta t\, \mathbf{B}(\mathbf{X}_P)\, \mathbf{v}^{\mathrm{e}}$$

where $\Delta\mathbf{e} = [\, \Delta\varepsilon_{xx}\ \Delta\varepsilon_{yy}\ \Delta\gamma_{xy}\,]^{\mathrm{T}} = \Delta t\, [\, d_{xx}\ d_{yy}\ d_{xy}\,]^{\mathrm{T}}$ or $\Delta\mathbf{e} = [\, \Delta\varepsilon_{xx}\ \Delta\varepsilon_{yy}\ \Delta\gamma_{xy}\ \Delta\varepsilon_{\Theta\Theta}\,]^{\mathrm{T}} = \Delta t\, [\, d_{xx}\ d_{yy}\ d_{xy}\ d_{\Theta\Theta}\,]^{\mathrm{T}}$ for the plane strain and axisymmetric problems, respectively. Then, stresses can be obtained from the constitutive relations.

The convective step consists of mapping of the velocity field from the material points to the computational grid which can remain in the same position as at the beginning of the time increment or can be changed. Nodal velocities

$$\mathbf{v} = [v_{1x}\ \ v_{1y}\ \ v_{2x}\ \ v_{2y}\ \ \ldots\ \ v_{nx}\ \ v_{ny}]^{\mathrm{T}}$$

are calculated from the equation [22–25]

$$\mathbf{M}\mathbf{v} = \mathbf{S}^{\mathrm{T}}\, \mathbf{M}_d\, \mathbf{V} \tag{11}$$

which expresses equivalence of momentum calculated for the material points and for the computational grid, where

$$\mathbf{V} = [V_{1x}\ \ V_{1y}\ \ V_{2x}\ \ V_{2y}\ \ \ldots\ \ V_{Nx}\ \ V_{Ny}]^{\mathrm{T}}$$

is the vector of velocities of all material points, and matrices $\mathbf{S}$ and $\mathbf{M}_d$ are defined as follows:

$$\mathbf{S} = \begin{bmatrix} \mathbf{N}(\boldsymbol{X}_1) \\ \mathbf{N}(\boldsymbol{X}_2) \\ \vdots \\ \mathbf{N}(\boldsymbol{X}_N) \end{bmatrix}, \quad \mathbf{M}_d = \begin{bmatrix} \mathbf{M}_1 & \mathbf{0} & \ldots & \mathbf{0} \\ \mathbf{0} & \mathbf{M}_2 & \ldots & \mathbf{0} \\ \vdots & \vdots & \ddots & \vdots \\ \mathbf{0} & \mathbf{0} & \ldots & \mathbf{M}_N \end{bmatrix}, \quad \mathbf{M}_i = \begin{bmatrix} M_i & 0 \\ 0 & M_i \end{bmatrix}$$

4.1. Time integration of constitutive relations

Using the forward-Euler rule of integration to the relation (1), we can write

$$\frac{1}{\Delta t}\,(\sigma_{ij}^{t+\Delta t} - \sigma_{ij}^{t}) = \overset{\nabla}{\sigma}_{ij} + \sigma_{ik}^{t}\,\dot{\omega}_{kj} + \sigma_{jk}^{t}\,\dot{\omega}_{ki}$$

and obtain stresses at time $t + \Delta t$ as the projection of elastic (trial) stresses

$$\sigma_{ij}^{\mathrm{e}} = \sigma_{ij}^{t} + \sigma_{ik}^{t}\,\Delta\omega_{kj} + \sigma_{jk}^{t}\,\Delta\omega_{ki} + A_{ijkl}\,\Delta\varepsilon_{kl}$$

where $\Delta\varepsilon_{ij} = \Delta t\, d_{ij}, \Delta\omega_{ij} = \Delta t\, \dot{\omega}_{ij}$, onto the set of plastically admissible stresses, B [5, 7, 8]

$$\sigma_{ij}^{t+\Delta t} = \begin{cases} \sigma_{ij}^{\mathrm{e}} & \text{if } \sigma_{ij}^{\mathrm{e}} \in B \\ \dfrac{m\,p^{\mathrm{e}}}{q^{\mathrm{e}}}\, s_{ij}^{\mathrm{e}} - p^{\mathrm{e}}\delta_{ij} & \text{if } \sigma_{ij}^{\mathrm{e}} \notin B \ \&\ p^{\mathrm{e}} > 0 \\ 0 & \text{if } \sigma_{ij}^{\mathrm{e}} \notin B \ \&\ p^{\mathrm{e}} \leqslant 0 \end{cases}$$

The above algorithm of integration of the constitutive relations is not incrementally objective, which means that it does not preserve the objectivity of the stress measure within a finite time

increment, although the objective measure of stress rate is used ($\overset{\nabla}{\sigma}_{ij}$). The incremental objectivity can be achieved by applying deformation- or rotation-neutralized formulation of the constitutive relations (see the paper by Saran and Runesson [36] and papers cited therein for details). In the present paper, the inaccuracy caused by the lack of incremental objectivity in the used integration rule is not significant as the small time increment is applied in the explicit procedure of solution to the dynamic equations.

4.2. Solution to the frictional contact problem

The variational formulation of the contact problem for deformable bodies leads to the implicit variational inequality, some terms of which are non-differentiable functionals (see e.g. [33, 37]), which makes the problem difficult to solve. To overcome these troubles, the penalty regularisation method can be used for the frictional constraints (2) and (3).

In the regularized form of the friction law, the relation between slip, v_T, and the tangential stress, σ_T, is similar to the constitutive relation for the elastic–plastic material (see e.g. [38–41]). The tangential velocity is the sum of the elastic and inelastic parts (v_T^{e} and v_T^{i}, respectively)

$$\dot{v}_T = \dot{v}_T^{\mathrm{e}} + \dot{v}_T^{\mathrm{i}}$$

$$\dot{v}_T^{\mathrm{e}} = -\frac{1}{c_T}\,\dot{\sigma}_T$$

$$\dot{v}_T^{\mathrm{i}} = \begin{cases} -\dot{\lambda}\,\dfrac{\sigma_T}{|\sigma_T|} & \text{if } f_c = 0 \\ 0 & \text{if } f_c \leqslant 0 \end{cases}$$

where $\dot{\lambda} \geqslant 0$, and c_T is the penalty parameter. The above relations are written for the two-dimensional case considered in the paper.

The relation between the normal components of velocity and contact stress does not have to be regularised because, in the case of a cohesionless granular material, the inequality $\sigma_N \leqslant 0$ is always true, and normal tractions at the nodes of the computational mesh can be calculated from the equations of motion by setting $v_N = 0$.

Unlike the constitutive relations which are satisfied at the material points, the relations related to the contact phenomenon are fulfilled at the nodes of the computational mesh. The contact problem is relatively easy to solve in the case of a mesh constant in time. The following algorithm of solving the frictional contact problem is applied. For each node of the computational mesh, located on the surface of an obstacle body (silo walls), the normal contact force (at time $t + \Delta t$) is obtained from the relation

$$F_{cN}^{t+\Delta t} = -F_N^{t+\Delta t} + R_N^{t+\Delta t}$$

which follows from the equation of motion (10) after using the condition $a_N^{t+\Delta t} = 0$. Then the following cases are considered:

I. Contact ($F_{cN}^{t+\Delta t} \leqslant 0$).

1. Sticking node. The trial value of the tangential force is calculated from the equation

$$F^{\mathrm{e}} = F_T^t - c_T\, v_T^{t+\Delta t}\, \Delta t$$

where $c_T > 0$ is the penalty parameter.

(a) If $|F^{\mathrm{e}}| \leqslant \mu |F_N^{t+\Delta t}|$, then $F_T^{t+\Delta t} = F^{\mathrm{e}}$ and the node is considered sticking in the next step.
(b) If $|F^{\mathrm{e}}| > \mu |F_N^{t+\Delta t}|$, then $F_T^{t+\Delta t} = (F^{\mathrm{e}}/|F^{\mathrm{e}}|)\mu\, |F_N^{t+\Delta t}|$ and the node is considered sliding in the next step.

2. Sliding node.

(a) If $v_t^t\, v_t^{t+\Delta t} > 0$, then $F_T^{t+\Delta t} = -(v_T^{t+\Delta t}/|v_T^{t+\Delta t}|)\mu |F_N^{t+\Delta t}|$ and the node is considered sliding in the next step.
(b) If $v_t^t\, v_t^{t+\Delta t} \leqslant 0$, then calculations are performed as in the case of a sticking node, but the trial tangential force is expressed as follows:

$$F^{\mathrm{e}} = -\frac{v_T^t}{|v_T^t|}\, \mu\, |F_N^{t+\Delta t}| - c_T\, v^{t+\Delta t}\, \Delta t$$

II. Separation ($F_{cN}^{t+\Delta t} = 0$). Set $F_{cT}^{t+\Delta t} = 0$. The node is considered sticking in the next step in the case of contact.

4.3. Stability

It should be pointed out that the particle-in-cell method in general may require the shorter time increment than the standard finite element method, where, in the case of one-dimensional element with linear shape functions, the condition of stability has the form [42]

$$\Delta t \leqslant \Delta t_{\mathrm{crit}}^{\mathrm{FE}} = \begin{cases} \dfrac{2}{\sqrt{3}}\, \dfrac{h}{C} & \text{for the consistent mass matrix (CMM)} \\ \dfrac{2}{\sqrt{2}}\, \dfrac{h}{C} & \text{for the lumped mass matrix (LMM)} \end{cases} \tag{12}$$

where h is the element size and C denotes the speed of elastic wave propagation. On the contrary to the finite element method, in the particle-in-cell method, the critical value of the time step depends on the mutual position of the material points and the computational element mesh. The required expression for the critical value of the time step can be derived from the stability condition (see e.g. [42])

$$\Delta t^2 \leqslant \frac{4m}{k} \tag{13}$$

where m and k are coefficients in the single homogeneous equation

$$m\ddot{u} + c\dot{u} + ku = 0$$

obtained as a result of modal decomposition of the dynamic system of equations. In one-dimensional case, for the linear element with one degree of freedom, we obtain the following expression for the diagonal term of the mass matrix:

$$m_{ii} = \begin{cases} \displaystyle\sum_{P=1}^{p_{\mathrm{e}}} M_P\, (\xi_P)^2 & \text{for CMM} \\ \displaystyle\sum_{P=1}^{p_{\mathrm{e}}} M_P\, \xi_P & \text{for LMM} \end{cases} \tag{14}$$

where $(1-\xi_P)h$ is the distance between the Pth material point and the ith node of the element, h denotes the length of the element, and p_e the number of material points in the element. In the case of linear elasticity, we can derive from equation $(9)_3$ the expression for the element stiffness matrix

$$\mathbf{k}^e = \sum_{P=1}^{p_e} M_P \, \mathbf{B}^T(\boldsymbol{X}_P) \frac{E}{\varrho} \mathbf{B}(\boldsymbol{X}_P) \tag{15}$$

and its diagonal term

$$k_{ii} = \sum_{P=1}^{p_e} M_P \left(\frac{C}{h}\right)^2 \tag{16}$$

where the relation $C^2 = E/\varrho$ is utilized. Applying equations (13)–(16), we obtain

$$\Delta t \leqslant \Delta t_{\text{crit}}^{\text{PIC}} = \begin{cases} 2\dfrac{h}{C}\sqrt{\left(\sum M_P\,(\xi_P)^2\right)/\left(\sum M_P\right)} & \text{for CMM} \\ 2\dfrac{h}{C}\sqrt{\left(\sum M_P\,\xi_P\right)/\left(\sum M_P\right)} & \text{for LMM} \end{cases} \tag{17}$$

The comparison of equations (12) and (17) shows that value Δt_{crit} may be significantly lower for PIC method than for FEM when the material points are located near one of the ends (or corners in the two-dimensional case) of the element. Equation (17) implies that a smaller number of material points in one element means a larger possibility that $\Delta t_{\text{crit}}^{\text{PIC}}$ is much smaller than $\Delta t_{\text{crit}}^{\text{FE}}$.

In the problem of silo discharging, the largest distortions of the flowing material are observed in the vicinity of the connection of a silo wall (or a silo bottom) with an outlet. This fact causes that, at some time instants, some elements located in this region contain a smaller number of material points than on the average. This implies the requirement of using the shorter time step in particle-in-cell analysis than in the finite element one.

4.4. Overall algorithm

The overall procedure, used to solve the considered dynamic problem, is outlined below.

1. Initializing state variables for material points—initial values are calculated in the static analysis. Initializing time value, $t := 0$.
   The initial fields of displacements and stresses are found by solving the quasi-static problem using the standard finite element method formulated in the updated Lagrangian description [7, 8].
2. Beginning of calculation for one time step. Finding velocities for grid nodes, $\mathbf{v}^t$, solving the system of equations (11)
$$\mathbf{M}^t \mathbf{v}^t = (\mathbf{S}^t)^T \mathbf{M}_d \mathbf{V}^t$$
3. Calculating the vector of nodal internal forces, $\mathbf{R}^t$,
$$\mathbf{R}^t = \sum_{P=1}^{N} M_P \, \mathbf{B}^T(\boldsymbol{X}_P^t)\, \mathbf{s}^{\varrho\, t}$$
4. Calculating the vector of nodal forces, $\mathbf{F}^t$, equivalent to gravitational forces, according to equation (9), and frictional forces, $\mathbf{F}_c^t$, according to Section 4.2.

5. Calculating the vector of nodal accelerations by solving the system of equations

$$\mathbf{M}^t \mathbf{a}^{t+\Delta t} = \mathbf{F}^t + \mathbf{F}_c^t - \mathbf{R}^t$$

6. Updating velocities of the material points

$$\mathbf{V}_P^{t+\Delta t} = \mathbf{V}_P^t + \Delta t\, \mathbf{N}(\mathbf{X}_P^t)\, \mathbf{a}^{t+\Delta t}, \quad P = 1, \ldots, N$$

7. Calculating the nodal velocities, $\mathbf{v}^L$, related to updated velocities of the material points, by solving the system of equations

$$\mathbf{M}^t \mathbf{v}^L = (\mathbf{S}^t)^{\mathrm{T}}\, \mathbf{M}_d \mathbf{V}^{t+\Delta t} \tag{18}$$

8. Calculating the strain increment and spin at each material point using vector $\mathbf{v}^L$. Update stresses $\boldsymbol{s}^{t+\Delta t}$ according to Section 4.1, and mass density

$$\varrho^{t+\Delta t} = (J_t^{t+\Delta t})^{-1}\, \varrho^t$$

where $J_t^{t+\Delta t}$ is the Jacobian of the deformation gradient related to the configuration at time t.

9. Updating position of the material points

$$\boldsymbol{X}_P^{t+\Delta t} = \boldsymbol{X}_P^t + \Delta t\, \mathbf{N}(\boldsymbol{X}_P^t)\, \mathbf{v}^L, \quad P = 1, \ldots, N$$

10. Setting $t := t + \Delta t$. Exiting the procedure if $t > T$ or going to point 2 otherwise.

In the above procedure, the nodal vector $\mathbf{v}^L$ is used in order to calculate stresses instead of $\mathbf{v}^t + \Delta t\, \mathbf{a}^{t+\Delta t}$. If the latter was used, some material points located near the free boundary would separate from the rest of the body. This is possible when the position of an only material point in an element approaches the element boundary, which implies that some terms of the element mass matrix tend to zero while the corresponding terms of the vector of nodal internal forces are constant. The use of vector $\mathbf{v}^L$ to calculate the stresses smoothes the field of accelerations—this procedure has been proposed by Sulsky *et al.* [24].

The theory of the particle-in-cell method (also called a material point method in [25]) described in Sections 3 and 4 (except Sections 4.1–4.3) is taken directly from [23–25].

5. NUMERICAL EXAMPLES

In the presented examples, the triangular element with linear shape functions is used. The initial (static) state has been calculated by the use of the updated Lagrangian formulation of the finite element method [7, 8] under the assumption that the gravitational forces are applied quasi-statically (the final load has been reached in five steps). This way of approximation of initial fields of displacements and stresses is very simple but it gives the interactions between the stored material and silo walls which are in good agreement with the Janssen formula [43], verified experimentally. The mesh generator described in [44] has been employed to prepare the geometrical data. Four material points of equal masses are introduced for any element of the mesh used in the quasi-static analysis (see Figure 1). The initial mesh applied in the quasi-static analysis is employed as the computational mesh in the dynamic calculations. Two types of material flow are considered—the funnel and mass ones. Both problems: the plane strain problem and the axisymmetric problem are illustrated in the examples.

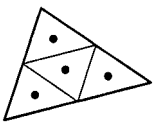

Figure 1. Division of triangular element and material points

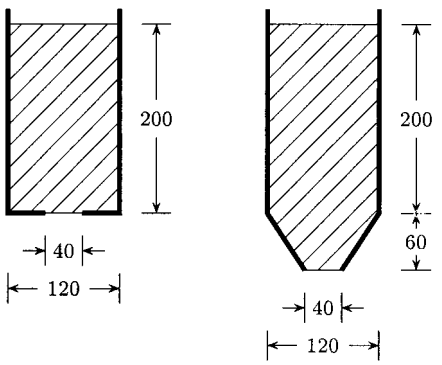

Figure 2. Cross-sections of silos—plane strain problem

Table I. Characteristics of computational meshes—plane strain problem

		Flat bottom			Trapezoidal hopper		
Mesh no.	Element size (m)	No. of nodes	No. of elements	No. of mat. points	No. of nodes	No. of elements	No. of mat. points
1	0·1	239	413	1480	272	469	1704
2	0·05	808	1489	5320	951	1755	6384
3	0·025	2949	5644	20344	3368	6446	23552

In the examples, calculations have been made with the following material data: $E = 1 \times 10^6$ Pa, $v = 0{\cdot}3$, $\varrho = 1500\,\mathrm{kg/m^3}$, $\varphi = 25°$, $\varphi_w = 20°$, where φ and φ_w denote the internal friction angle and the angle of friction between the granular material and silo walls. The penalty coefficient, c_T, has been chosen as 1×10^7 N/m^3.

5.1. Plane strain problem

The silos of the two shapes presented in Figure 2 are considered: the first one with a flat bottom, and the second one with a trapezoidal hopper. The dimensions shown in the figure are given in centimeters.

As the cross-sections of each silo is symmetric, only half of its area has been analysed. Calculations have been made for three element meshes characterised in Table I. The node located at the corner of the flat bottomed silo has been assumed to be fixed.

The values of the time increment, applied for all the used computational meshes, are presented in Table II.

Table II. Values of time increment—plane strain problem

Mesh no.	Time increment (s)	
	Flat bottom	Trapezoidal hopper
1	1×10^{-3}	1×10^{-3}
2	5×10^{-4} for $t \leqslant 3$ and $2{\cdot}5 \times 10^{-4}$ for $t > 3$	5×10^{-4}
3	$2{\cdot}5 \times 10^{-4}$ for $t \leqslant 2$ and $1{\cdot}25 \times 10^{-4}$ for $t > 2$	$2{\cdot}5 \times 10^{-4}$

The results of the computations: the deformation of the material and the wall tractions are shown in Figures 3 and 4 for several time instants. In order to get clear visualisation of the obtained flow pattern, the initial configuration of the body has been divided into 16 layers, and the material points belonging to odd layers (counting from the top) have been drawn in the figures. The presented results have been obtained for the densest meshes (No. 3 in Table I) which are also depicted in the figures. Wall tractions are measured in Pa; normal and tangential tractions are plotted in thick and thin lines, respectively. The funnel flow is observed in the case of the silo with the flat bottom, and the mass flow in the case of the trapezoidal hopper. In the case of funnel flow, the change of sign of tangential tractions along the vertical wall appears in the vicinity of stagnant zone in the corner of the silo due to unloading of the bottom part of the material during the discharging process.

The flow rate of the material has been calculated for three meshes utilized in the analysis. In the case of funnel flow, the numerical results have been compared with the result obtained from the empirical formula established by Beverloo *et al.* [45]:

$$W = 45\,\varrho\,A'\,\sqrt{g\,D'_{\mathrm{h}}} \tag{19}$$

where W is measured in g/min, A' is the effective orifice area, measured in cm^2 and related to the effective hydraulic diameter D'_{h}, measured in cm, g the gravitational constant, measured in $\mathrm{cm/s}^2$. The effective hydraulic diameter is expressed by the hydraulic diameter, D_{h}, and the diameter of material grains, d, $D'_{\mathrm{h}} = D_{\mathrm{h}} - 1{\cdot}4\,d$. For the plane flow, the following formula can be derived from equation (19):

$$W' = 45\sqrt{2g}\,\left[D\left(1 - 0{\cdot}7\frac{d}{D}\right)\right]^{1{\cdot}5}$$

where W' denotes the flow rate for the unit length of the outlet measured in the direction perpendicular to the cross-section, D is the width of the outlet. The diagram of the obtained flow rate, W', is shown in Figure 5, and compared with the empirical values, calculated for three ratios d/D: 0, 0·1 and 0·2. Good consistency of the results is observed for the time interval when the flow rate is nearly stabilized. The method exhibits the faster convergence in the case of mass flow where the material flow is less distorted.

In the case of funnel flow, the analysis of the discharging process lasting 2·5 s needed 17·43 h of computation time. In the case of mass flow, the obtained total discharging time is 3·09 s—the computation time was 19·48 h. The computations were made on the Silicon Graphics (MIPS R5000 Indy A2) workstation.

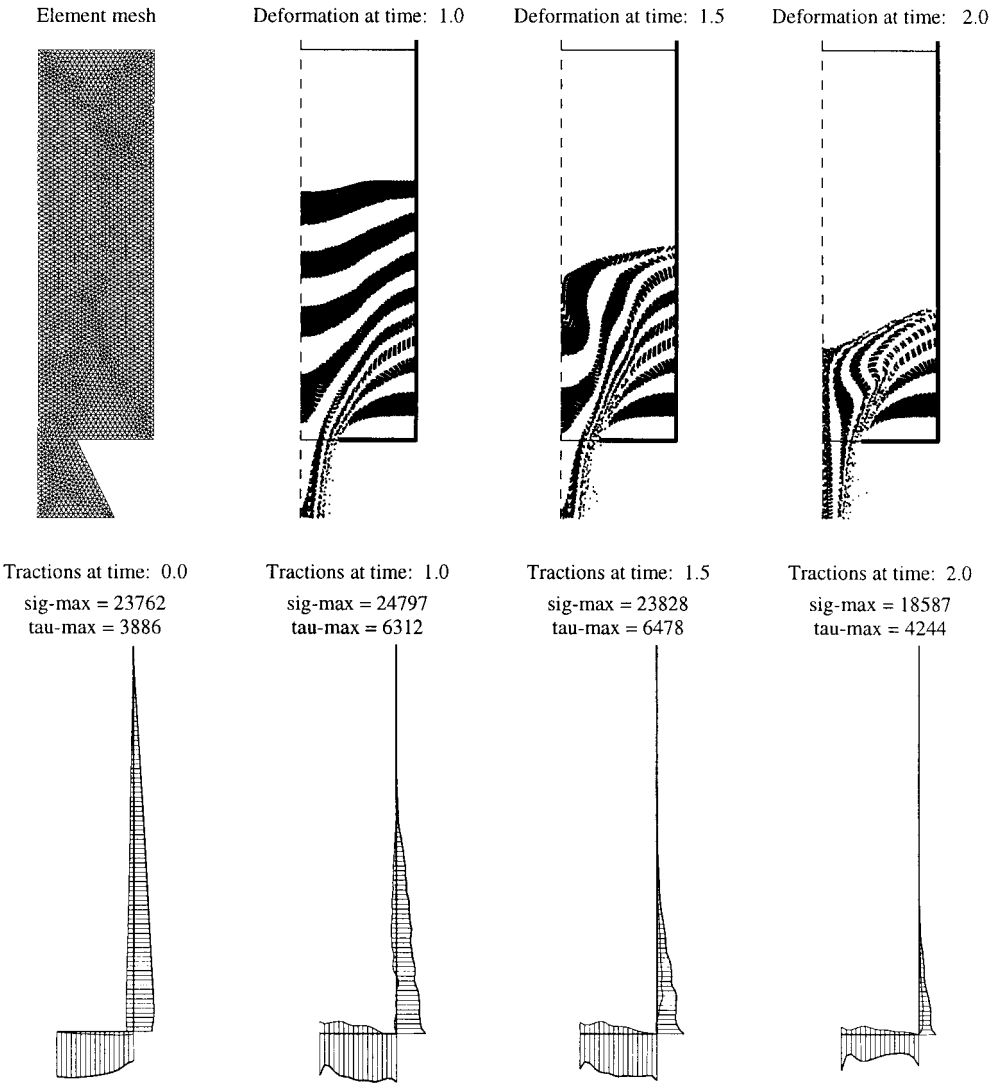

Figure 3. Deformation and tractions—plane strain problem, funnel flow

5.2. *Axisymmetric problem*

As in the previous example, two silos of different shapes are considered in the case of axisymmetric flow: the first one with a flat bottom, and the second one with a conical hopper. The cross-sections of the silos are presented in Figure 6, where the dimensions are given in centimeters.

Calculations have been made for half of the region using three element meshes characterised in Table III.

The values of the time increment applied for all the used computational meshes are presented in Table IV.

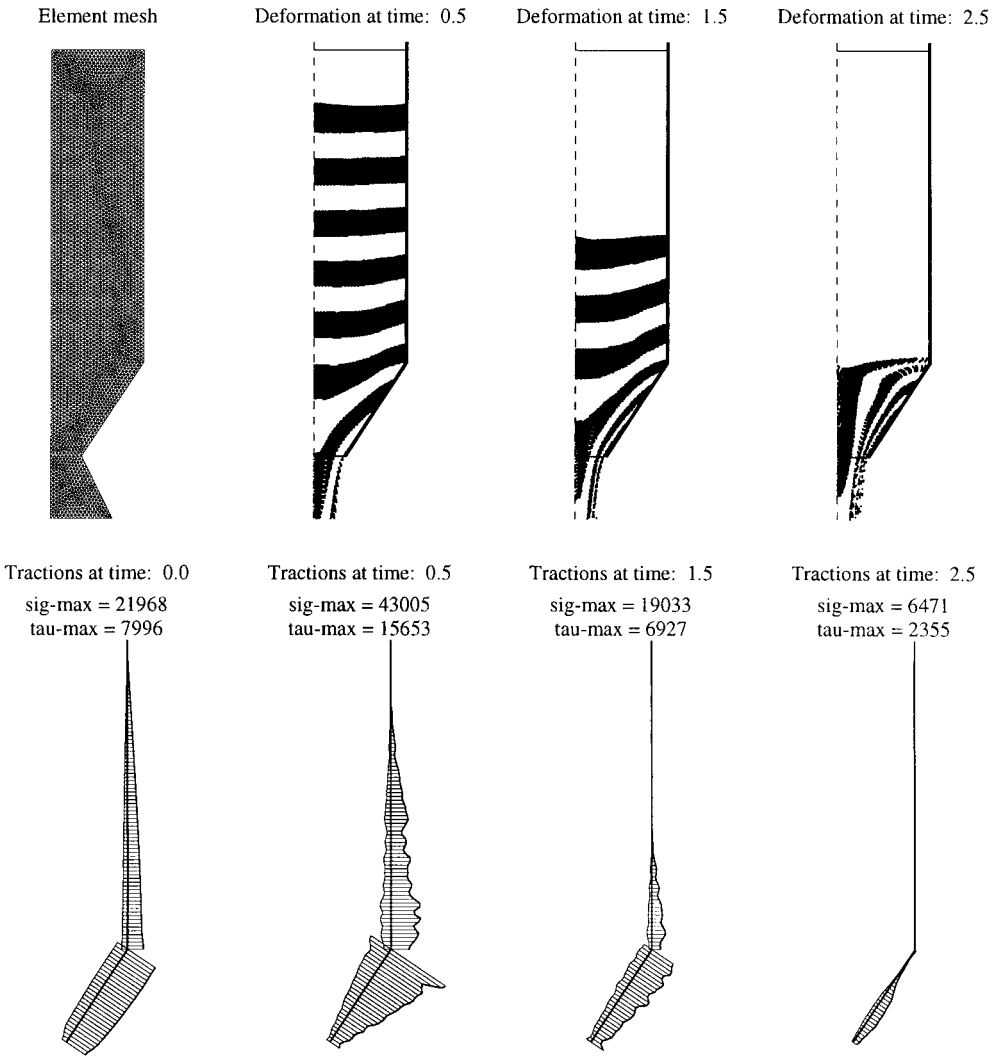

Figure 4. Deformation and tractions—plane strain problem, mass flow

Table III. Characteristics of computational meshes—axisymmetric problem

		Flat bottom			Conical hopper		
Mesh no.	Element size (mm)	No. of nodes	No. of elements	No. of mat. points	No. of nodes	No. of elements	No. of mat. points
1	12·5	351	625	2224	421	752	2732
2	6·25	1300	2447	8776	1563	2947	10776
3	3·125	4470	8640	30912	5466	10580	38672

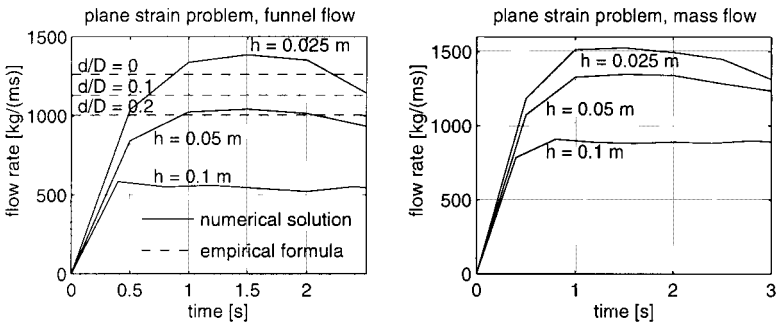

Figure 5. Flow rate diagrams—plane strain problem

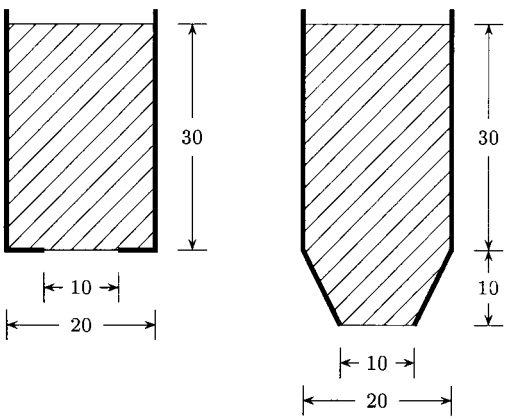

Figure 6. Cross-sections of silos—axisymmetric problem

Table IV. Values of time increment—axisymmetric problem

	Time increment (s)	
Mesh no.	Flat bottom	Conical hopper
1	10×10^{-5}	10×10^{-5}
2	5×10^{-5}	5×10^{-5}
3	$2{\cdot}5 \times 10^{-5}$ for $t \leqslant 1{\cdot}0$ and $1{\cdot}25 \times 10^{-5}$ for $t > 1{\cdot}0$	$2{\cdot}5 \times 10^{-5}$ for $t \leqslant 1{\cdot}2$ and $1{\cdot}25 \times 10^{-5}$ for $t > 1{\cdot}2$

The deformation of the flowing material and corresponding wall tractions obtained for the densest meshes are presented in Figures 7 and 8. The results show, especially those related to funnel flow, that the particle-in-cell method can handle such phenomena as large slippage and self-collision of the granular body without difficulty.

The flow rate diagrams are shown in Figure 9 for all the meshes used in the computations. In the case of funnel flow, the results are compared with the empirical prediction given by Beverloo

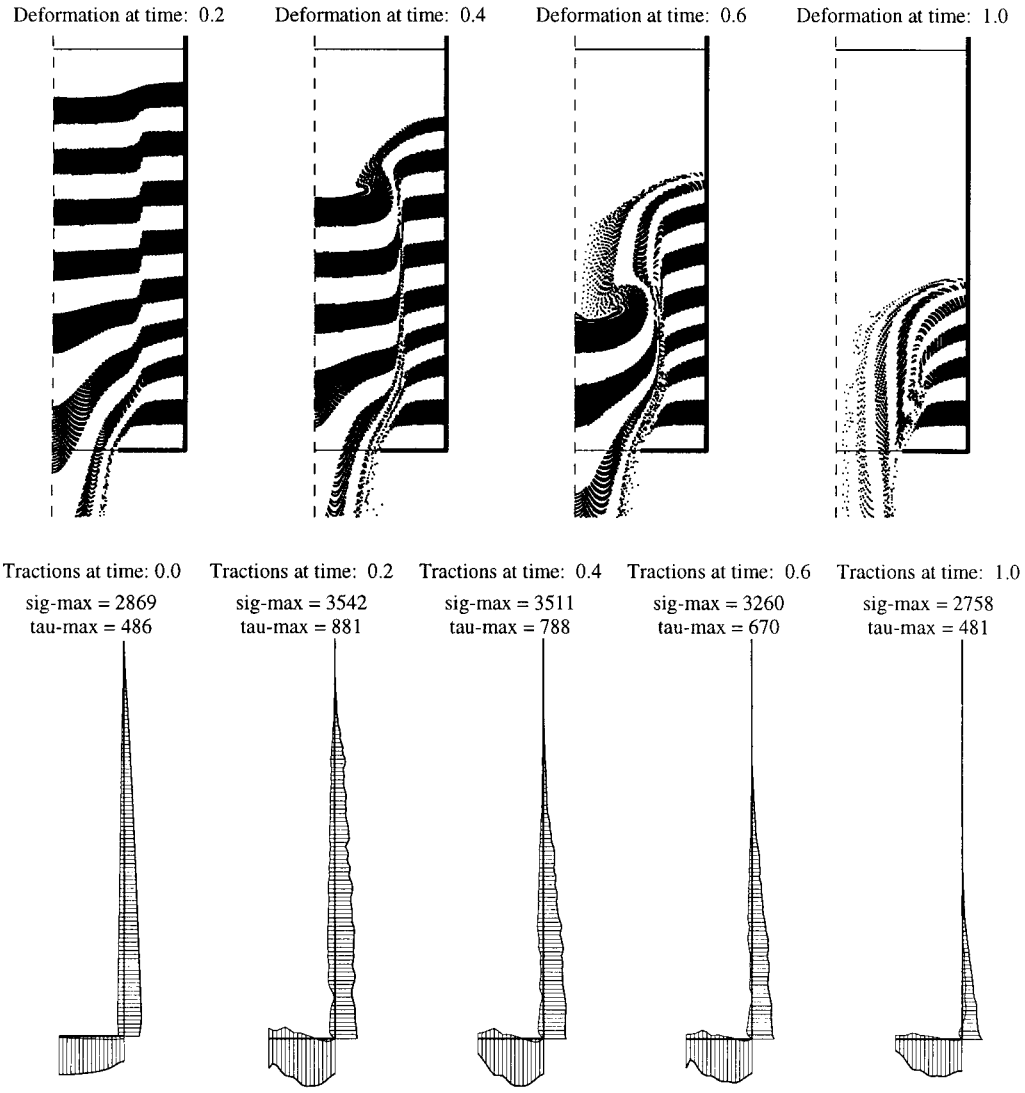

Figure 7. Deformation and tractions—axisymmetric problem, funnel flow

et al. [45] which, in the case of axisymmetric flow, has the following form:

$$W = 35\varrho\sqrt{g}\left[D_0\left(1 - 1{\cdot}4\frac{d}{D_0}\right)\right]^{2{\cdot}5} \tag{20}$$

where D_0 denotes the diameter of the silo outlet. The axisymmetric flow is more distorted than the plane flow and its analysis need much denser mesh and more material points—a low rate of convergence is observed, in particular in the case of the funnel flow. The value of flow rate obtained for the densest mesh is about 25 per cent less than the value obtained from (20) for the ratio $d/D = 0$.

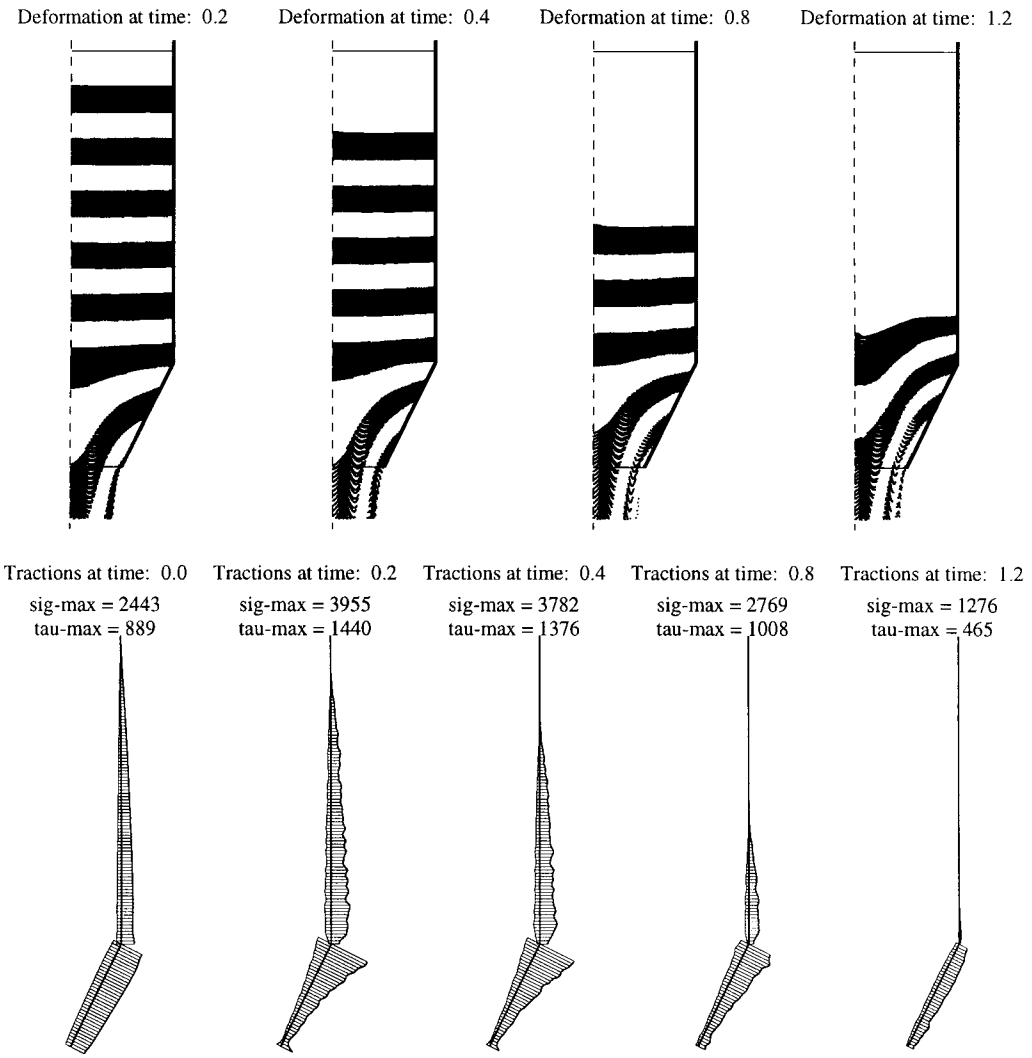

Figure 8. Deformation and tractions—axisymmetric problem, mass flow

The computation time was 105·1 h in the case of funnel flow—2 s of real discharging process were analysed. In the case of mass flow, the discharging process of 1·4 s duration needed 83·3 h of computation time.

5.3. Plane strain problem—comparison of PIC and UL FE methods

The comparison of results obtained by the PIC method and the updated Lagrangian formulation of the finite element method with mesh re-zoning [7, 8] has been made for the plane flow of the granular material in the silo, the cross-section of which is presented in Figure 10. Calculations have been made under the assumption that there is no friction between the stored material and

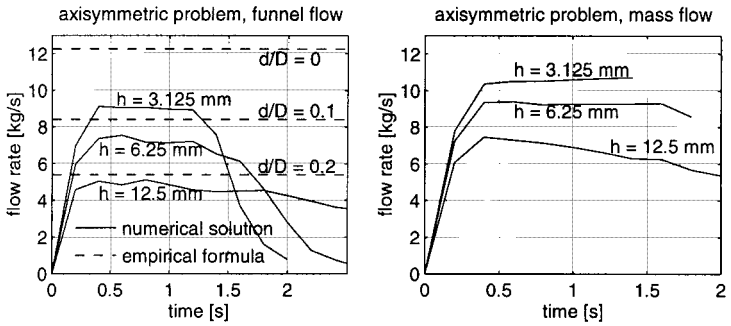

Figure 9. Flow rate diagrams—axisymmetric problem

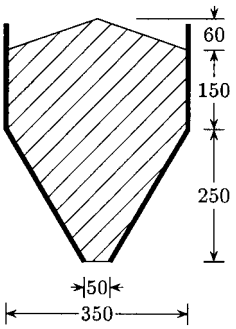

Figure 10. Cross-sections of a silos—plane strain problem

silo wall—the case when the updated Lagrangian formulation with mesh re-zoning appears to be reliable. In the case of the UL FE method, half of the region occupied by the material has been divided into 730 six-node isoparametric elements—1537 nodes have been introduced. The element mesh has been re-zoned 13 times. In the case of the PIC method, a computational mesh with 2876 three-node elements and 1523 nodes has been applied, and 11 056 material points have been used. Calculations have been made with the time increment set as 0·01 and 0·001 s for the UL FE and PIC methods, respectively. The Newmark time integration algorithm has been used in the FE calculations with parameters $\delta = 0{\cdot}5$, $\alpha = 0{\cdot}25$.

The comparison of deformations obtained using the two methods are shown in Figure 11. The similarity of shapes of the upper free surface of the material can be observed. Slower flow has been obtained by the UL FE method than by the PIC one. The total discharging time is equal 7·90 and 7·13 s according to the results obtained by means of the UL FE and the PIC methods, respectively.

6. CONCLUSIONS

The particle-in-cell method has been applied to the problem of motion of a granular material during the process of discharging a silo. The plane and axisymmetric flows have been analysed. The mass and funnel types of flow have been investigated. The equations of motion and the

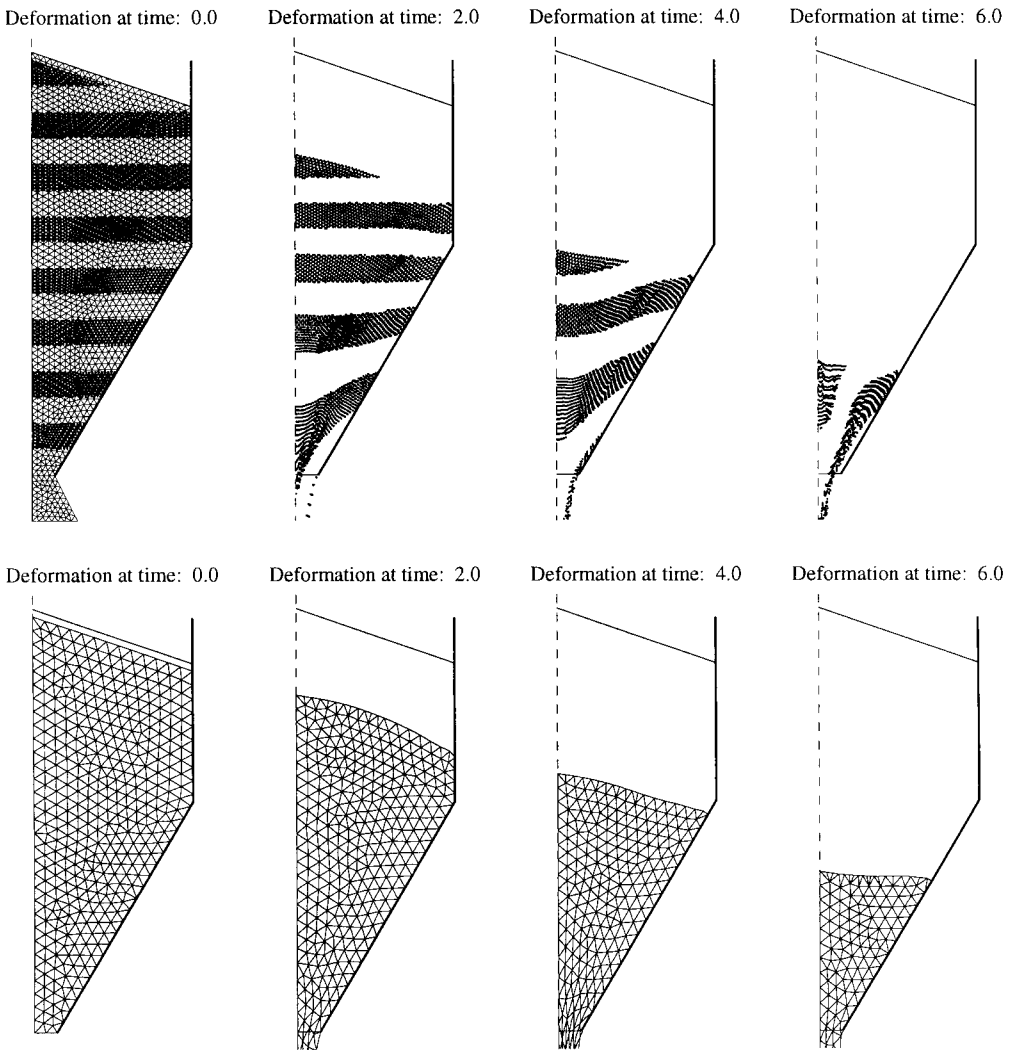

Figure 11. Deformation obtained by PIC and UL FE methods—plane strain problem

frictional contact problem have been solved using the computational mesh, constant in time, while the history of state variables has been tracked at the material points. The triangular element with linear shape functions has been utilised. The dynamic problem has been solved by an explicit method. It has been shown that the method gives a possibility to simulate the entire discharging process, and handles problems of large slippage and self-collision of the granular material without difficulty. However, the rate of convergence of the method is rather low, especially in the case of axisymmetric flow. In order to improve the efficiency of the method, such measures as the implementation of an implicit scheme of time integration of the equations of motion, the use of elements with shape functions of higher order, adaptive techniques, and parallel computation should be considered.

The elastic–plastic material model of the Drucker–Prager type, used in the present analysis, is very simple and does not include such an important effect as the dependence of tangential moduli on the current stress state. Other, more realistic constitutive models of the granular material (e.g. elastic–plastic model with two yield surfaces proposed by Lade [46] or generalized hypo-elastic or hypo-plastic model proposed by Kolymbas [30, 31] and Wu and Bauer [32]) need to be implemented in future studies of the problem.

ACKNOWLEDGEMENTS

The first author thanks the Korea Science and Engineering Foundation for the financial support in the framework of the Post-doctoral Fellowship Program for Foreign Researchers.

REFERENCES

1. Jenike AW, Shield RT. On the plastic flow of Coulomb solids beyond original failure. *Journal of Applied Mechanics* 1959; **26**:599–602.
2. Walters JK. A theoretical analysis of stresses in axially-symmetric hoppers and bunkers. *Chemical Engineering Science* 1973; **28**:779–789.
3. Eibl J, Rombach G. Numerical investigation on discharging silos. In *Proceedings of the 6th International Conference on Numerical Methods in Geomechanics*, Swoboda G (ed.) Balkema, 1988; 317–320.
4. Häussler U, Eibl J. Numerical investigation on discharging silos. *Journal of Engineering Mechanics* ASCE 1984; **110**:957–971.
5. Runesson K, Nilsson L. Finite element modelling of the gravitational flow of a granular material. *International Journal of Bulk Solids Handling* 1986; **6**:877–884.
6. Klisiński M, Runesson K, Więckowski Z, Hermansson E. Modelling of flow of bulk materials in silos. *Proceedings of Conference on Reliable Flow of Particulate Solids II*, Oslo, August 1993.
7. Wieckowski Z. Finite deformation analysis of motion of bulk material in Silo. Application of finite element method. *Research Report*, Luleå University of Technology, Division of Structural Mechanics, 1994.
8. Więckowski Z, Klisiński M. Finite deformation analysis of motion of granular materials in a silo. *Archives of Mechanics* 1995; **47**:617–633.
9. Langston PA, Tüzün U, Heyes DM. Continuous potential discrete particle simulations of stress and velocity fields in hoppers: transition from fluid to granular flow. *Chemical Engineering Science* 1994; **49**:1259–1275.
10. Langston PA, Tüzün U, Heyes DM. Discrete element simulation of granular flow in 2D and 3D hoppers: dependence of discharge rate and stress on particle interactions. *Chemical Engineering Science* 1995; **50**:967–987.
11. Nayroles B, Touzot G, Villon P. Generalizing the finite element method: diffuse approximation and diffuse elements. *Computational Mechanics* 1992; **10**:307–318.
12. Libersky LD, Petschek AG, Carney AG, Hipp TC, Allahdadi FA. High strain Lagrangian hydrodynamics—a three-dimensional SPH code for dynamic material response. *Journal of Computational Physics* 1993; **109**:67–75.
13. Belytschko T, Lu YY, Gu L. Element-free Galerkin methods. *International Journal for Numerical Methods in Engineering* 1994; **37**:229–256.
14. Liu WK, Jun S, Li S, Adee J, Belytschko T. Reproducing kernel particle methods for structural dynamics. *International Journal for Numerical Methods in Engineering* 1995; **38**:1655–1679.
15. Chen JS, Pan C, Wu CT, Liu WK. Reproducing kernel particle methods for large deformation analysis of non-linear structures. *Computer Methods in Applied Mechanics and Engineering* 1996; **139**:195–227.
16. Duarte CA, Oden JT. An h-p adaptive method using clouds. *Computer Methods in Applied Mechanics and Engineering* 1996; **139**:237–262.
17. Liszka TJ, Duarte CAM, Tworzydło WW. hp-Meshless cloud method. *Computer Methods in Applied Mechanics and Engineering* 1996; **139**:263–288.
18. Oñate E, Idelsohn S, Zienkiewicz OC, Taylor RL, Sacco C. A stabilized finite point method for analysis of fluid mechanics problems. *Computer Methods in Applied Mechanics and Engineering* 1996; **139**:315–346.
19. Johnson GR, Stryk RA, Beissel SR. SPH for high velocity impact computations. *Computer Methods in Applied Mechanics and Engineering* 1996; **139**:347–373.
20. Randles PW, Libersky LD. Smoothed particle hydrodynamics: some recent improvements and applications. *Computer Methods in Applied Mechanics and Engineering* 1996; **139**:375–408.
21. Harlow FH. The particle-in-cell computing method for fluid dynamics. In *Methods for Computational Physics*, vol. 3, Adler B, Fernbach S, Rotenberg M (eds). Academic Press: New York, 1964; 319–343.

22. Burgess D, Sulsky D, Brackbill JU. Mass matrix formulation of the FLIP particle-in-cell method. *Journal of Computational Physics* 1992; **103**:1–15.
23. Sulsky D, Chen Z, Schreyer HL. A particle method for history-dependent materials. *Computer Methods in Applied Mechanics and Engineering* 1994; **118**:179–196.
24. Sulsky D, Zhou SJ, Schreyer HL. Application of a particle-in-cell method to solid mechanics. *Computer Physics Communication* 1995; **87**:236–252.
25. Sulsky D, Schreyer HL. Axisymmetric form of the material point method with applications to upsetting and Taylor impact problems. *Computer Methods in Applied Mechanics and Engineering* 1996; **139**:409–429 .
26. Donea J. Arbitrary Lagrangian–Eulerian finite element methods. In *Computational Methods for Transient Analysis*, Belytschko T, Hughes TJR (eds). Elsevier Science Publisher: Amsterdam, 1983; 473–516.
27. Lehmann T. Einige Bemerkungen zu einer allgemeinen Klasse von Stoffgesetzen für große elasto-plastiche Formänderungen. *Ingenieur-Archiv* 1972; **41**:297–310.
28. Johnson GC, Bamman DJ. A discussion of stress rates in finite deformation problems. *International Journal of Solids and Structures* 1984; **20**:725–737.
29. Benson DJ. Computational methods in Lagrangian and Eulerian hydrocodes. *Computer Methods in Applied Mechanics and Engineering* 1992; **99**:235–394.
30. Kolymbas D. Generalized hypoelastic constitutive equation. In *Constitutive Equations for Granular Non-Cohesive Solids*, Saada AS, Bianchini G (eds). Balkema: Rotterdam, 1988; 349–359.
31. Kolymbas D. An outline of hypoplasticity. *Ingenieur-Archiv* 1991; **61**:143–151.
32. Wu. W, Bauer E. A simple hypoelastic constitutive model for sand. *International Journal for Numerical and Analytical Methods in Geomechanics* 1994; **18**:833–862.
33. Duvaut G, Lions JL. *Les inéquations en mécanique et en physique*. Dunod: Paris, 1972.
34. Adams RA. *Sobolev Spaces*. Academic Press: New York, 1975.
35. Panagiotopoulos PD, *Inequality problems in Mechanics and Applications. Convex and Non-Convex Energy Functions*. Birkhauser: Boston, 1985.
36. Saran MJ, Runesson K. A generalized closest-point-projection method for deformation-neutralized formulation in finite strain plasticity. *Engineering Computations* 1992; **9**:359–370.
37. Kikuchi N, Oden JT. *Contact Problems in Elasticity: A Study of Variational Inequalities and Finite Element Methods*. SIAM: Philadelphia, 1988.
38. Laursen TA, Simo JC. A continuum-based finite element formulation for the implicit solution of multibody, large deformation frictional contact problems. *International Journal for Numerical Methods in Engineering* 1993; **36**:3451–3485.
39. Michałowski R, Mróz Z. Associated and nonassociated sliding rules in contact friction problems. *Archives of Mechanics* 1970; **30**:259–276.
40. Wriggers P, Vu Van T, Stein E. Finite element formulation of large deformation impact–contact problem with friction. *Computers and Structures* 1990; **37**:319–331.
41. Zhong ZH, *Finite Element Procedures for Contact-Impact Problems*. Oxford University Press: New York, 1993.
42. Zienkiewicz OC, Taylor RL. *The Finite Element Method*. (4th edn), vol. 2. McGraw-Hill: London, 1991.
43. Janssen HA. Versuche über Getreidedruck in Silozellen. *Zeitschrift des Verein der Deutsche Ingenieure*, 1895; **39**:1045–1049.
44. Klisiński M, Mesh generator based on ring type of advancing front. *Report*, Luleå University of Technology, 1994.
45. Beverloo WA, Leniger HA, van de Velde J. The flow of granular solids through orifices. *Chemical Engineering Science* 1961; **15**:260–269.
46. Lade VP, Elastic–plastic stress–strain theory for cohesionless soil with curved yield surface. *International Journal of Solids and Structures* 1977; **13**:1019–1035.

